A Multistranded Polymer Model Explains MinDE Dynamics in *E. coli* Cell Division

Eric N. Cytrynbaum and Brandon D. L. Marshall
Department of Mathematics, University of British Columbia, Vancouver, British Columbia, Canada

ABSTRACT In *Escherichia coli*, the location of the site for cell division is regulated by the action of the Min proteins. These proteins undergo a periodic pole-to-pole oscillation that involves polymerization and ATPase activity of MinD under the controlling influence of MinE. This oscillation suppresses division near the poles while permitting division at midcell. Here, we propose a multistranded polymer model for MinD and MinE dynamics that quantitatively agrees with the experimentally observed dynamics in wild-type cells and in several well-studied mutant phenotypes. The model also provides new explanations for several phenotypes that have never been addressed by previous modeling attempts. In doing so, the model bridges a theoretical gap between protein structure, biochemistry, and mutant phenotypes. Finally, the model emphasizes the importance of nonequilibrium polymer dynamics in cell function by demonstrating how behavior analogous to the dynamic instability of microtubules is used by *E. coli* to achieve a sufficiently rapid timescale in controlling division site selection.

INTRODUCTION

Escherichia coli bacteria undergo division by pinching in half at the midpoint of the long axis of their cylindrical form. At the onset of this process, FtsZ, a bacterial homolog of tubulin, localizes to the inner membrane forming a polymer ring at midcell called the Z-ring. Along with a suite of other proteins, the Z-ring contracts, pinching the cell in two (see (1) for a recent review). The Z-ring is localized to midcell by the combined efforts of two independent pathways that suppress its polymerization elsewhere. The first pathway is DNA-dependent and leads to the suppression of Z-ring formation in the regions immediately surrounding each of the two replicated and segregated chromosomes that sit on either side of the cell midplane. This leaves both the midcell and polar regions eligible for Z-ring formation (2). Polar division leads to asymmetric daughter cells, one containing two chromosomes and the other chromosome-less, and is referred to as a minicell phenotype. These polar divisions are usually suppressed in wild-type cells by the second pathway, the Min protein system—MinC, MinD, and MinE. MinC is responsible for interfering with Z-ring formation (3,4). MinD is an ATPase that localizes to the membrane in the ATP-bound form (5) and recruits MinC (6). MinE controls the spatial localization of MinD along the membrane (5) by inducing the ATPase activity of MinD (7). By restricting MinD and hence MinC to the polar regions, MinE spatially regulates the inhibition of division to the poles leaving only the midcell region available for Z-ring formation.

In *E. coli*, MinD and MinE act in a dynamic oscillatory manner that is independent of MinC (8). MinD first attaches to the inner cell membrane at one of the cell's two poles (8), then polymerizes in a tightly coiled helix extending from the originating pole almost to midcell (9). Subsequently, MinE attaches to MinD at the midcell end of the helix forming what was originally referred to as an E-ring (10), although a more recent microscopy study indicated that it might be better described as an E-helix (9). Upon attachment, MinE induces the ATPase activity of MinD (11), which drives the leading edge of the MinD helix back toward the pole. The E-ring progresses back toward the pole, clearing MinD as it goes (12,13). MinD then reattaches at the opposite pole, repeating this pattern many times throughout the cell cycle with a period of ~40 s (8,13).

Several mathematical models have been proposed to explain the MinDE oscillations as the spontaneous result of an instability of a homogeneous protein distribution (14–23). The strength of these models lies in their simplicity and the elegance of pattern formation from a two-protein system. From a theoretical perspective, these models have relied on Turing-like instabilities or Cahn-Hilliard-type phase separation.

A fundamental difficulty with this pattern-formation paradigm lies in the assumption that MinD forms an unstructured aggregate. There are only ~2000 MinD monomers that must cover nearly half the cell surface (24). To do so as an unstructured aggregate, the mean spacing between monomers would be ~10 times the size of a single MinD protein, a fact poorly accounted for by the use of continuous densities as in most earlier models. To account for this low density regime, several proposed models have treated all proteins as discrete molecules that interact stochastically (18,21,23). Interestingly, spontaneous pattern formation (SPF) is still possible in this regime.

However, through the use of deconvolution microscopy, MinD has been observed to form a single helical structure several microns in length extending from pole to midcell (9) rather than forming a uniformly distributed aggregate as

Submitted September 11, 2006, and accepted for publication April 23, 2007.
Address reprint requests to E. N. Cytrynbaum, E-mail: cytryn@math.ubc.ca.
Editor: Gaudenz Danuser.

0006-3495/07/08/1134/17 $2.00
doi: 10.1529/biophysj.106.097162

originally thought (8,13). From experimental observations (25) as well as theoretical considerations discussed later in this article, the MinD helix most likely consists of a single double-stranded filament. As far as modeling is concerned, there seems to be a tradeoff between SPF and generating the helical structure of membrane-bound MinD in the sense that none of the existing models has been capable of explaining both phenomena. Continuum-description models do not resolve submicron structure and hence cannot predict the observed helical structure (17,20). Models that incorporate the polymer nature of membrane-bound MinD have operated in parameter regimes that lead to short length distributions of polymers, thereby allowing SPF but failing to display the helical structure (22,23).

Drew et al. (26) proposed a polymer model wherein turnover is restricted to the polymer tip, as expected for multistranded filaments. Their model assumed nucleation of polymers at the poles but by describing the helix as a population density of polymers, unnecessary and unrealistic assumptions were required to ensure oscillations. The helical structure is not an emergent feature of the model but is implicitly assumed to be a feature of a bundle of filaments whose persistence length and elastic properties lead it to bend into a coiled structure on the membrane. The drawback of such a modeling approach, which we nonetheless adopt here, is that spatial pattern formation is not explained but assumed; the benefit is that it allows an exploration of how various phenotypes that have not been addressed by previous modeling efforts might be explained by a polymer model.

As an extension of the work of Drew et al. (26), we revisit the polymer paradigm in an effort to explain several phenotypes with a particular focus on MinE mutants. First, we propose a mechanism for the polar bias in polymer nucleation, which allows for an explanation of the *minE*$^-$ mutant. Although this mutant is easily explained by several of the SPF models, it poses challenges for any polymer model which assumes the presence of a dedicated nucleation sites allowing nucleation of only a single polymer per pole. The mechanism we suggest relies on the biophysics of lipid domains in a manner motivated by previous hypotheses (27). The explanation of the *minE*$^-$ mutant that this mechanism admits essentially depends on two key generic features, described in The Model, below. The specific mechanism we propose, while certainly not incontrovertible, provides a biophysically reasonable demonstration of these generic features.

Interestingly, the experiments that motivate the proposed nucleation mechanism pose a major challenge to the SPF models. In particular, domains of distinct lipid composition containing a high concentration of the anionic phospholipid cardiolipin have been observed at the poles of *E. coli* cells (28). Furthermore, a mutant lacking the cationic phospholipid phosphatidylethanolamine, having a membrane composed only of the anionic phospholipids phosphatidylglycerol and cardiolipin, was shown to have a loss of specificity in the localization of MinD, instead showing randomly scattered MinD foci (29). This observation suggests that these lipid domains may play a role in polymer nucleation. This PE$^-$ phenotype was ostensibly explained by Fange and Elf (30) using a stochastic variation on the Huang model; however, to explain the PE$^-$ mutant, the parameter values required for the MinD binding kinetics and membrane diffusion in mutant cells were several orders-of-magnitude out of reasonable ranges (29,31). In particular, the mutant MinD-membrane-binding rate constant was taken to be four orders-of-magnitude smaller than that of wild-type cells, despite experimental evidence that the binding affinity is actually higher (29). In addition, the mutant membrane-bound diffusion coefficient for MinD was assumed to be two orders-of-magnitude lower than the value assumed for wild-type cells, which at 10^{-2} μm^2/s is already on the low end of what has been observed for transmembrane proteins (which MinD is not). The physical basis for such extreme assumptions is unclear.

In addition to the polar nucleation model, which provides an explanation for the *minE*$^-$ mutant, we propose a polymer model that relies on detailed structural and biochemical data and elucidates the behavior of several other mutant phenotypes. Under reasonable simplifying assumptions, the model admits a closed-form solution providing a handle on parameter dependence and allowing for quantitative validation against experimental data (8). The model also allows testing of the role and importance of cooperativity, which has been reported in both MinD polymerization (11,32) and MinE-induced hydrolysis (11,25). Finally, the model allows for comparison with the many reported *min* mutant phenotypes including deletion of *minE*, overexpression of *minD* and *minE* in various combinations and at various expression levels, and three different truncations of the MinE protein also at various expression levels. The proposed explanations of the truncation mutants are the first to appear in the modeling literature and the fitting of the overexpression mutant data represent the first demonstration of quantitative agreement between a model and experiments for these Min phenotypes.

From a more broad perspective, the model elucidates the role of nonequilibrium polymer dynamics in bacterial cell function. In the eukaryotic context, dynamic instability of microtubules has been shown to play vital roles in temporally sensitive tasks in cell division and other important cell functions (33). Here, we suggest that the MinD and MinE proteins together demonstrate behavior directly analogous to dynamic instability of microtubules and that this behavior is crucial to achieving Z-ring suppression at a sufficiently rapid rate.

THE MODEL

MinD dimer cycling and strain

We begin with a model of MinD dimer cycling, which has the requisite features to explain the MinE-dependence of polymer nucleation. Upon binding ATP, cytosolic MinD forms dimers (34) that attach to the inner surface of the cytoplasmic

membrane (11,35). Countering the MinD dimerization process, MinE also forms dimers in the cytosol (36) which can attach to the membrane-bound MinD dimers and induce hydrolysis, thereby driving them off the membrane (11,25) by a previously described mechanism (37,38). Once in the cytosol, ADP is exchanged for ATP and the process can repeat. This cycle is illustrated in Fig. 1 *B*.

We propose that this dimerization cycle is spatially regulated in the cell so as to facilitate nucleation exclusively at the pole in the following way (see Fig. 1 *C*). Suppose that MinD-ATP dimers spontaneously bind in a strained conformation to membrane under high tension but, for membrane under low tension, this strain is relieved by membrane deformation. Furthermore, we assume that both strain and MinE attachment are required for inducing hydrolysis. One possible explanation for the strain requirement is that the strain is needed to close the dimerization face around the two ATPs, a conformation change that is thought to be an important step in the activation of several members of the structurally analogous ATPase family to which MinD belongs (39). Another possibility is that deformation associated with the strain might be required to allow MinE to bind, a scenario that is more consistent with the details of the calculation of the polar nucleation bias given in Results.

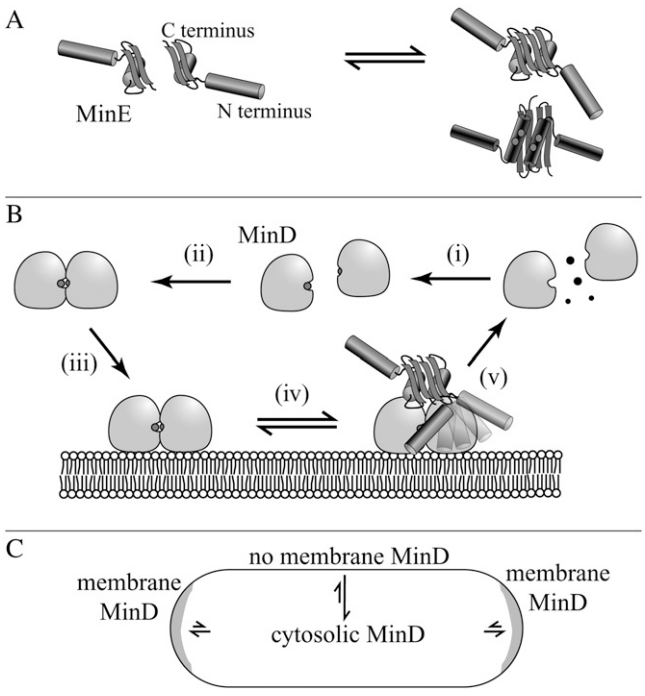

FIGURE 1 Proposed dimer model. (*A*) MinE undergoes dimerization. The N-terminus anti-MinD domain is involved in inducing hydrolysis by MinD and the C-terminus is involved in dimerization and E-ring formation. Residues 45 and 49, involved in E-ring formation, are shown as light patches on the underside of the MinE dimer. (*B*) MinD cycles from the cytosol where it binds ATP (*i*), dimerizes (*ii*), attaches to the membrane (*iii*), recruits MinE (*iv*), hydrolyzes ATP, and is released from the membrane (*v*). MinE is proposed to undergo a conformation change in which the anti-MinD domain moves to the MinD dimerization face (*v*) simultaneously blocking polymerization of dimers and inducing MinD ATPase activity. (*C*) If MinD attaches at the poles, hydrolysis and release is assumed to be slower leading to an accumulation of dimers at the pole.

From where does this hypothesis of strain in the dimer arise? In an in vitro membrane-binding assay, Hu et al. (11) found that MinD-ATP, upon binding to lipid vesicles, was capable of distorting spherical vesicles of diameter 0.1–2 μm into elongated tubes several microns in length with an approximate radius of 25 nm. Furthermore, from diffraction patterns of cryo-EM images of tubes, they observed that MinD formed a lattice encircling the tubes on the outside with a lateral spacing of approximately the width of a MinD monomer. This suggests that upon attaching to lipid vesicles, not only does MinD-ATP form a polymer structure but this structure has an energetic preference to take on a curved conformation when attached to membrane. In other words, membrane-associated MinD polymerization provides a force with which membrane is deformed and a membrane tube is pulled from a vesicle, a phenomenon similar to that observed for dynamin (40) and microtubules (41) as well as studied with techniques using glass beads (42).

The details of this in vitro observation allow estimation of the energy associated with dimer strain. We assume the following time course for the vesicle tubulation phenomenon, illustrated in Fig. 2. At sufficiently high concentrations of MinD, a polymer forms on the surface of the vesicle, pinching out a tube, thereby removing any slack in the membrane. Based on the extent of tubulation observed (11), we further assume that MinD is capable of pulling the membrane tube into the regime in which the membrane is stretched.

The calculation described in the Appendix indicates that, when attached to a membrane under high tension that does not easily submit to deformation, a MinD polymer would be forced to deform and can store $>7\ k_BT$ per dimer as internal mechanical strain. We assume that the strain is present at the dimer level.

As a caveat, we note that this tension mechanism is based on calculations from an in vitro system, which differs from the in vivo context in that it is free of a cell wall and cytoskeletal proteins. Although our estimate of the strain energy in vitro is quite large, as discussed in Results, even if the in vivo figure is half as much, the polar nucleation bias would still be sufficient.

The important features of this mechanism, required for consistency with the *minE*$^-$ mutant described later, are that MinD attaches to the membrane everywhere and that MinE is only effective at removing it from the membrane away from the poles due to some feature of the membrane at the poles, decreased tension associated with the polar lipid domains being the candidate proposed here, as discussed in the next section.

Polar nucleation of MinD polymers

Domains of distinct lipid composition have been observed at the poles of wild-type *E. coli* cells (28), and recently these

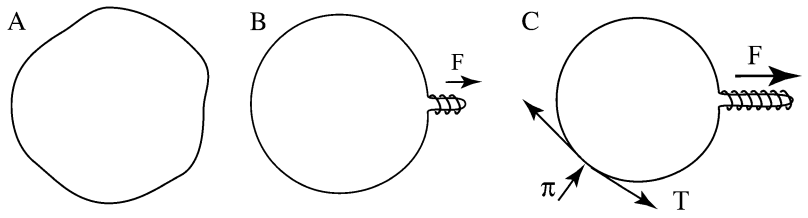

FIGURE 2 Progression of vesicle tubulation. (*A*) MinD binds to a slack vesicle, (*B*) begins to polymerize thereby pulling out any extra membrane, and (*C*) eventually stretches the membrane as the membrane/polymer tube grows. In panel *B*, the force $F \approx 0$–3 pN is opposed mostly by membrane bending. In panel *C*, the force $F \approx 10$ pN is opposed by the membrane tension (T), which is assumed to be in mechanical equilibrium with the osmotic pressure (π) induced by volume change.

structures have been analyzed theoretically (43). In principle, membrane tension could be reduced within these domains due to the line tension along their periphery (44). The corresponding slower rate of hydrolysis inside the domains would lead to an accumulation of dimers and therefore a much increased probability of nucleating a MinD helix at the poles compared to elsewhere on the membrane, as is characteristic of wild-type cells (8). Calculations presented in Results demonstrate that under these assumptions, a lack of strain at the poles leads to at least a two order-of-magnitude difference in the polymer nucleation rate at the poles compared with elsewhere on the membrane.

In addition to being relegated to the poles, nucleation is cooperative in the sense that the polymer nucleation rate is proportional to D^n, where D is the cytosolic concentration of MinD and $n = 3$ or 4. Here we are assuming that the MinD helix is formed by a single double-stranded polymer, an assumption justified by concentration and geometric constraints (see the Appendix). This nonlinear nucleation probability is typical of multistranded polymers (e.g., $n = 3$ or 4 for actin filaments (45), $n \sim 12$ for microtubules (46)). Cooperativity of this type has been observed in in vitro MinD-membrane-binding assays (11,32).

This cooperativity means that as a MinD polymer is disassembling at one end, a polymer can only form at the other pole once a sufficient fraction of the polymer has disassembled, an important feature for maintaining the asynchrony of polymer growth at either pole. Also, the delay between disassembly at one end and assembly at the other means that both diffusion and ATP-ADP exchange have a significant period of time over which to occur, up to half of the oscillation period, so it is reasonable to assume that both are quasi-steady processes with respect to assembly and disassembly dynamics (see the Appendix for details).

Another important feature of nucleation is that once a first polymer forms at one pole, other polymers are inhibited from forming at the same pole due the membrane tension induced by the growth of the first polymer. This is explicitly represented in the equations presented below by the dependence of the dimer hydrolysis rate on the polar membrane tension. Once a first polymer forms at a pole, we assume that it locally increases the membrane tension in the polar domain by deforming the membrane as a result of its preferred curvature. This polymer-dependent increase in tension introduces strain in the surrounding membrane-bound dimers leading to their MinE-mediated removal from the membrane preventing further nucleation.

MinE and E-ring formation

MinE monomers have three distinct structural features that are important in the discussion of their role in division site selection: the anti-MinD domain, the dimerization residues, and the topological specificity residues (all depicted in Fig. 1). The anti-MinD domain sits at the N-terminus of the protein (residues 1–32) and consists primarily of an α-helix. It is known to be necessary and sufficient for driving MinD from the membrane (47,48). Dimerization depends on the interaction of several portions of the C-terminus domain of the protein (residues 33–88) which together form a β-sheet and coiled-coil in the assembled dimer (49). Finally, the topological specificity (TS) residues, 45 and 49, are required for MinE to selectively target its anti-MinD activity to MinD in the midcell region. Loss of these residues leads to a failure to form the E-ring (24). We assume these residues play a role in binding of MinE to membrane-bound MinD, as suggested by Shih et al. (9). This assumption is also supported by evidence that when the anti-MinD domain is prevented from binding to MinD, MinE is still capable of binding to membrane-bound MinD, despite being incapable of inducing ATPase activity (50). Based on the location of the TS residues on the C terminus α-helices (light patches on the underside of MinE in Fig. 1 *A*) (49) and a matching of the geometries of the MinD and MinE dimers, their binding is assumed to occur as depicted in Figs. 1 and 3.

An important issue to address is the mechanism by which MinE influences the ATPase activity of MinD dimers. In comparison with a structurally analogous ATPase involved in nitrogen fixation (NifH), MinD is missing an α-helix at the edge of its dimerization face (39) (see Fig. 3 *B*). Here, we propose that this missing α-helix is required for ATP hydrolysis and is replaced in the MinD context by the anti-MinD domain of MinE. This idea is consistent with the finding that the anti-MinD domain interacts with the so-called α-7 helix (*yellow α-helix* in Fig. 3 *B*) (51) and that mutations in α-4 (*green α-helix* in Fig. 3 *B*) and α-7 suppress the influence of MinE on MinD ATPase activity (50,52). (This α-helix nomenclature is adopted from (53).) Thus, our suggestion for MinE-coenzyme function is that upon attaching to MinD, the anti-MinD domain of MinE must

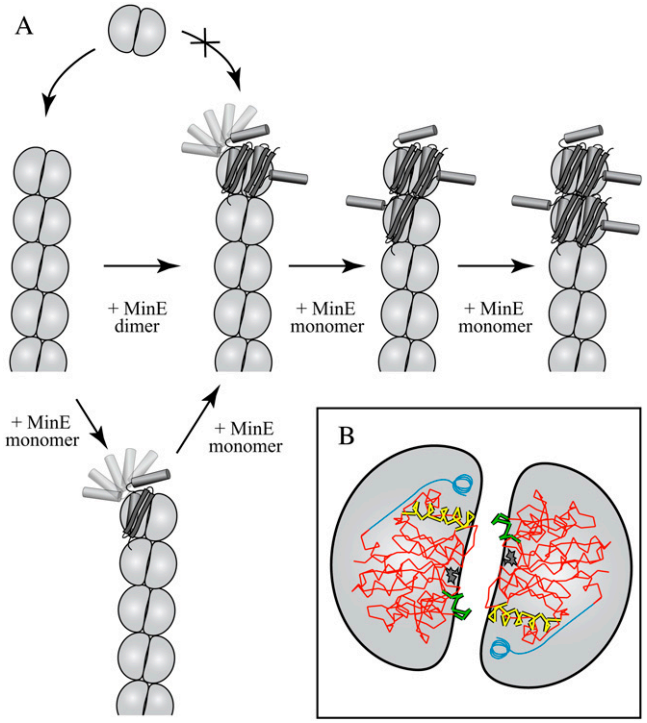

FIGURE 3 E-ring formation and function. (*A*) E-ring nucleation by two pathways: sequential monomer binding or dimer binding. The monomer pathway is less preferred than the dimer pathway due to the extra intermediate step during which hydrolysis could lead to a loss of MinD subunits and MinE monomer at the tip. As a result, with a cytosolic dimerization dissociation constant of $K_E = 0.6\ \mu M$, nucleation is unlikely below that concentration and more likely above it. Finally, once MinE is attached at the tip, MinD is prevented from binding by the anti-MinD domain halting further polymerization. (*B*) Top view of the MinD dimer structure proposed in Lutkenhaus and Sundaramoorthy (39) superimposed on the cartoon shape of MinD. ATP are in dark shading. The α-helices α-4 and α-7, known to influence the anti-MinD activity of MinE, are in green and yellow, respectively (51,52). Note how the α-4 and α-7 domains from opposite monomers come together when the dimer forms. The blue α-helix is present in the structure of the analogous ATPase NifH but is missing from MinD (39). We propose that the anti-MinD domain of MinE takes its place.

rotate into place near the dimerization face and, by interacting with α-4 and α-7, induces hydrolysis (see Fig. 1 *v*). Finally, cytosolic MinE monomers and dimers are both assumed to be capable of clearing the nonpolar membrane of MinD dimers, an assumption implicitly required for oscillations. The MinE dimer structure does not seem necessary for this membrane clearing activity, based on the fact that a truncated form of MinE that is missing the dimerization domain is nonetheless capable of inducing MinD-ATP hydrolysis (47).

The next important issue to address is the manner in which MinE affects the MinD polymer, which generally ceases growth and begins disassembly at its midcell tip upon formation of the E-ring (12,13). In vitro studies have shown that MinE is capable of forming tetramers in solution with a dissociation constant of 2 mM (36). In vivo, we propose that MinE polymer formation is facilitated at lower concentration by the framework of the MinD polymer to which MinE can attach. Thus, we describe the E-ring as a ''retrograde'' double-stranded polymer that sits on top of the MinD polymer. E-ring formation guarantees that disassembly of the MinD polymer is processive—as a MinD dimer hydrolyzes its ATP and falls off the membrane, the next MinE down the line rotates its anti-MinD domain into place. The E-ring treadmills back along the MinD helix, both preventing further growth through steric exclusion by the anti-MinD domain and inducing disassembly. The nucleation of such a structure has been suggested previously to explain the cooperativity of MinD hydrolysis-induction (11).

In principle, the E-ring could nucleate at any point along the MinD polymer through attachment of monomers via their TS residues. However, the added affinity for MinD provided by the anti-MinD domain biases E-ring formation to the tip of the MinD polymer, the only location at which α-7 is accessible to the anti-MinD domain (see Fig. 3). Furthermore, even if an E-ring did form away from the tip, hydrolysis-induction would be prevented by steric exclusive of the α-7 by the neighboring subunits.

There are two pathways by which the E-ring can nucleate at the tip, either by sequential binding of two monomers or by the binding of a single dimer. The monomer pathway can be interrupted either by spontaneous dissociation of the first MinE monomer or by its induction of hydrolysis by its MinD host, which would lead to its own release. In contrast, the dimer pathway does not have this intermediate limiting step but instead requires dimerization in the cytosol before attaching to the tip. In either case, it can be argued that both tip-binding pathways, including the addition of a third monomer, occur at a rate proportional to the cube of the cytosolic monomer concentration but with different coefficients. Because of the limiting intermediate step in the monomer pathway, we argue that the monomer pathway is marginal and so omit it from the model. Cooperativity of MinE ATPase induction has been observed in vitro (11,25) and we infer that it is of the second type—cooperativity through cytosolic dimerization rather than facilitated binding to the MinD polymer.

This argument means that E-ring nucleation awaits the arrival of sufficient MinE dimers in the cytosol. Zhang et al. (36) measured an in vitro dissociation constant for dimerization of $K_E = 0.6\ \mu M$, well within the dynamic in vivo range. We therefore propose that the cytosolic concentration of MinE dimers is dynamically controlled during the MinDE oscillations so that E-ring nucleation happens after the MinD polymer grows far enough toward midcell to inhibit polar division. This control is accomplished by sequestration of cytosolic MinE in the E-ring attached to the older disassembling MinD polymer.

To summarize, suppose that one MinD polymer is already capped by an E-ring and a second polymer has just formed. As a MinD-MinE dimer pair pop off the tip of the first polymer, the liberated MinD, after ATP-ADP exchange, can incorporate into the nascent polymer but is blocked from

incorporating into the older disassembling polymer by the anti-MinD domain at its newly exposed tip. But why should the liberated MinE dimer rebind to the same E-ring (E-ring treadmilling) and not contribute to the formation of an E-ring on the nascent second polymer? This question is important because, if it did, the nascent polymer would be capped early, allowing for assembly of the division apparatus near the pole and hence minicelling. Because an E-ring already exists on the older polymer, much of the cytosolic pool of MinE is sequestered in that ring and the cytosolic concentration is low, in particular below K_E, so that most of the cytosolic pool is in monomer form. Monomers do not initiate E-rings but they can readily elongate existing ones, an important feature of multistranded polymers (54). It is only when the E-ring covers the length of the shrinking MinD polymer that monomers can no longer add to it, leading to a rise in the total cytosolic MinE concentration and in turn the dimer concentration. This finally triggers E-ring nucleation on the nascent polymer. This behavior, combined with the cooperativity of MinD polymer nucleation, is the source of stable asynchrony in the MinDE oscillations.

The analogy between E-ring formation and microtubule catastrophe is worth emphasizing at this point. By forming an E-ring rather than just continually attacking MinD from the cytosol, MinE can switch a MinD polymer from a growth state to a processive disassembly state. This analog of microtubule catastrophe allows for a rapid and precise covering of the half-cell and hence efficient prevention of Z-ring formation at the poles. These features of speed and spatial accuracy are similar to the search-and-capture of chromosomes in the division of eukaryotic cells (33,55).

Equations and parameters

In this section we present a system of equations describing the quantitative features of the model that we subsequently break into subsystems based on timescales. In the end, we arrive at a quasi-static dimer-cycling subsystem and a slower polymerization subsystem, which is implemented in two ways. The first is stochastic and is solved computationally, and the other is deterministic and can be solved analytically under certain simplifying assumptions. Solutions are described in Results.

The equations are

$$\frac{d}{dt}D_m = \frac{V}{A_m}k_{on}D_2 - (k_{hyd}E_2 + k_{hyd_0})D_m,$$
$$\frac{d}{dt}D_{pl} = \frac{V}{A_p}k_{on}D_2 - (k_{hyd}\,g(T_l)\,E_2 + k_{hyd_0})D_{pl},$$
$$\frac{d}{dt}D_{pr} = \frac{V}{A_p}k_{on}D_2 - (k_{hyd}\,g(T_r)\,E_2 + k_{hyd_0})D_{pr},$$
$$\frac{dl_D}{dt} = \delta(\chi_l k_{poly}D - (1-\chi_l)\Theta(l_D)k_{dep}),$$
$$\frac{dr_D}{dt} = \delta(\chi_r k_{poly}D - (1-\chi_r)\Theta(r_D)k_{dep}),$$
$$\frac{dl_E}{dt} = \delta(k^E_{poly}E\Theta(l_D - l_E) - k_{dep})(1-\chi_l)\Theta(l_E),$$
$$\frac{dr_E}{dt} = \delta(k^E_{poly}E\Theta(r_D - r_E) - k_{dep})(1-\chi_r)\Theta(r_E),$$

where Θ is the Heaviside function and all variables and parameters are described in Tables 1 and 2, respectively. Equations for D and E are not required because they can be calculated by conservation,

$$D + 2D_2 + 2(A_mD_m + A_pD_{pl} + A_pD_{pr})/V + (l_D(t) + r_D(t))/(\delta V) = D_{tot},$$
$$E + 2E_2 + (l_E + r_E)/(\delta V) = E_{tot},$$

where $D_2 = D^2/K_D$ and $E_2 = E^2/K_E$ are the MinD and MinE dimer concentrations, respectively, assumed to be in quasi-static equilibrium. The values χ_l and χ_r are discrete variables that switch between 0 and 1 as described below.

To summarize the equations above, MinD dimers attach to the membrane at a rate k_{on}. They detach from the membrane at a background rate k_{hyd_0}, and at a rate proportional to MinE: $k_{hyd}\,g(T)\,E_2$. The MinE rate is modulated by the factor $g(T)$, which depends on the local tension in the membrane. This factor is taken to be 1 whenever there is tension in the membrane (away from the poles or at the poles when a polymer is present) and $e^{-\Delta G}$ otherwise, where ΔG is the MinD strain energy required to allow MinE to bind to MinD. A MinD polymer grows at a rate proportional to the cytosolic MinD monomer concentration when not capped by an E-ring and disassembles at a constant rate once an E-ring has formed. We assume that cytosolic diffusion is fast compared to the timescale of polymer turnover. Because we will assume that the dimer kinetics are fast, assumptions about membrane-bound diffusion are not required although the details of the polymerization rates might vary slightly depending on the details assumed. Such subtleties ought not to change the basic results presented here.

Transitions between the deterministic dynamics of polymer growth and polymer disassembly (MinD nucleation: $\chi = 0 \rightarrow \chi = 1$ and E-ring formation: $\chi = 1 \rightarrow \chi = 0$) can

TABLE 1 Table of variables, with definitions

Name	Description	Units
D, D_2	Cytosolic concentration of MinD monomers, dimers	# per μm^3
D_m	Nonpolar membrane-bound concentration of MinD dimers	# per μm^2
D_{pl}, D_{pr}	Polar membrane-bound concentration of MinD dimers (left, right)	# per μm^2
E, E_2	Cytosolic concentration of MinE monomers, dimers	# per μm^3
l_D, r_D	Arclength of MinD helix (left, right)	μm
l_E, r_E	Arclength of MinE helix (left, right)	μm
χ_l, χ_r	State of MinD polymer ($\chi = 1$: growing, no E-ring, $\chi = 0$: capped by E-ring or completely disassembled)	—

TABLE 2 Table of parameters

Parameter	Description	Value	Source
k_{on}, k_{hyd}	Dimer on rate constant; MinE-induced MinD-dimer hydrolysis rate	—	Assumed to be fast relative to other processes.
k_{hyd_0}	Background MinD dimer hydrolysis rate	$k_{hyd}/10$	Hu et al. (11).
k_{dep}	E-ring-induced MinD hydrolysis rate	80 s^{-1}	Estimated from Hale et al. (13).
k_{poly}	MinD polymerization rate constant	100 μM^{-1} s^{-1}	Estimated from Hale et al. (13).
k_{poly}^{E}	E-ring elongation rate constant	160 μM^{-1} s^{-1}	Estimated from Hale et al. (13).
k_{nuc}	MinD polymer nucleation rate constant	0.001–0.1 μM^{-3} s^{-1}	Tested range; see text.
k_{cap}	E-ring initiation rate constant	0.06–1.5 μM^{-3} s^{-1}	Tested range; see text.
K_E	MinE dimer dissociation constant	0.6 μM	Zhang et al. (36).
D_{tot}	Total MinD concentration	4 μM	Estimated from Shih et al. (24) and de Boer et al. (35).
E_{tot}	Total MinE concentration	3 μM	Estimated from Shih et al. (24).
D_{thresh}	Threshold MinD concentration	1.5–3 μM	Hu et al. (11).
E_{thresh}	Threshold MinE concentration	2.5 μM	Fitted parameter; see text.
δ	Half MinD monomer length	2.5 nm	Suefuji et al. (25).
L, r, V	Cell length, radius, volume	3 μm, 3/8 μm, 1.3 μm^3	Approximate dimensions.
A_p, A_m	Polar and nonpolar surface areas	1 μm^2, 10 μm^2	Approximate dimensions.
θ	MinD helix pitch angle	80°	Estimated from Shih et al. (9).
λ	Phage expression level	3.3 μM	Fitted parameter; see text.

Parameters used in the deterministic and stochastic versions of the model. A more detailed discussion of parameter values is provided in the Appendix.

be treated in two ways, one stochastic and the other deterministic.

Under the assumption that the dimer kinetics are fast compared to the polymerization phenomenon, the dimer equations are assumed to be in a quasi-steady state relative to the polymer length equations. Nucleation proceeds by two membrane-bound dimers forming a tetramer or by a monomer adding to a membrane-bound dimer. Thus, nucleation is ultimately proportional to D^n where $n = 3$ or 4. E-ring formation is similar, being proportional to E^m where $m = 3$ or 4. So the stochastic implementation of the model treats MinD nucleation and E-ring formation as stochastic events with instantaneous probability densities $k_{nuc}D^n$ and $k_{cap}E^m$, respectively. Formally, this means that at any moment, a value of $\chi = 0$ associated with a polymer of zero length can switch to a value of $\chi = 1$ with probability $k_{nuc}D^n$ and hence start the polymer growing. Similarly, a value of $\chi = 1$ associated with a growing polymer can switch to a value of $\chi = 0$ with probability $k_{cap}E^m$, thereby initiating an E-ring and MinD polymer disassembly. Although the nonlinear probabilities (n, $m = 3$ or 4) are more realistic, we also examined the linear cases (n, $m = 1$) to explore the importance of the cooperativity that arises through dimerization. Cases $\{n = 3, m = 3\}$, $\{n = 1, m = 3\}$, and $\{n = 3, m = 1\}$ are all described in Results.

A deterministic approximation of the stochastic case, treating nucleation and capping as strongly cooperative events, was also analyzed. In this case, changes in the value of χ from 0 to 1 or from 1 to 0 occur at the precise moment that the MinD or MinE concentrations, respectively, rises above a critical level. Thus as the cytosolic MinD concentration rises above a critical level, D_{thresh}, an empty pole spontaneously nucleates a polymer. Similarly, if the cytosolic MinE dimer concentration surpasses a critical value, E_{thresh}, a growing polymer is capped with an E-ring. Under the assumption that both MinD and MinE polymer growth are rate-limited by the supply of monomers, the equations are solvable in closed form (see the Appendix).

RESULTS

Dimer cycling and polar nucleation

From the monomer and dimer equations, we can calculate the ratio of nonpolar/polar nucleation probabilities when one of the poles is polymer-free,

$$\frac{P_m}{P_p} = \frac{A_m D_m^{\frac{n}{2}}}{A_p D_p^{\frac{n}{2}}} = \frac{A_m}{A_p}\left(\frac{A_p}{A_m}\frac{k_{hyd}\, g(T)\, E_2 + k_{hyd_0}}{k_{hyd}\, E_2 + k_{hyd_0}}\right)^{\frac{n}{2}}$$
$$\sim \left(\frac{A_p}{A_m}\right)^{\frac{n}{2}-1}\left(\frac{k_{hyd_0}}{k_{hyd}\, E_2}\right)^{\frac{n}{2}} \sim \frac{1}{100},$$

where the first approximation relies on the observation (7) that $k_{hyd}\, E_2 \sim 10 k_{hyd_0}$ and the prediction from the strain model that $g(T) \ll 1$. The second approximation uses the conservative estimates that the polar lipid domain is $\sim 1/10$ of the total surface area, that again $k_{hyd}\, E_2 \sim 10 k_{hyd_0}$ and $n = 3$. Thus, when there is no tension at one of the poles, nucleation is 100 times more likely at that pole than elsewhere in the cell. Note that the ratio of background to MinE-induced hydrolysis was measured for polymerized MinD rather than for dimers so it is possible that due to difficulty of accessing the α-7 domain of MinD in polymer form, the relevant ratio for isolated dimers is even smaller than $1/10$. A nucleation exponent of $n = 4$ and a smaller ratio of membrane areas are also possible, all of which could lead to a ratio of nucleation probabilities that is smaller by several orders of magnitude.

MinDE oscillations

In the deterministic implementation of the model, two relevant solutions can be calculated. Provided $D_{tot} - D_{thresh} > E_{tot} - E_{thresh}$, a stable oscillatory solution reminiscent of wild-type oscillations can be found (see the Appendix and Fig. 4). This condition is equivalent to enforcing that the MinD nucleation threshold must be reached before the E-ring forming threshold is reached as a MinD polymer and E-ring disassemble. When this condition is not satisfied, a purely cytosolic state prevails—MinD polymers are capped and disassembled before they even have a chance to grow—and a minicell phenotype is predicted. In Fig. 4, this condition is illustrated by the fact that the nucleation threshold is higher than the capping threshold (shown graphically in terms of polymer length instead of cytosolic concentration).

When the oscillation condition holds, the period of the oscillations is given by $T = 2V(D_{tot} - 2(E_{tot} - E_{thresh}))/k_{dep}$ (see the Appendix). Interestingly, this expression demonstrates that the timescale of the process is determined solely by the disassembly rate, E-ring initiation threshold, total concentrations and cell size, but not the nucleation threshold nor the assembly dynamics. The latter two parameters only determine the fraction of the oscillation period that the polymer spends growing.

With parameter values as given in Table 2, the oscillation condition is satisfied and the predicted oscillation period is 45 s, roughly consistent with observations (8,13). Not appearing in the expression for the period, D_{thresh} is only restricted to a broad range of values by the oscillation condition, 0–3.5 μM, consistent with in vitro evidence that places it in the range 1.5–3 μM (11).

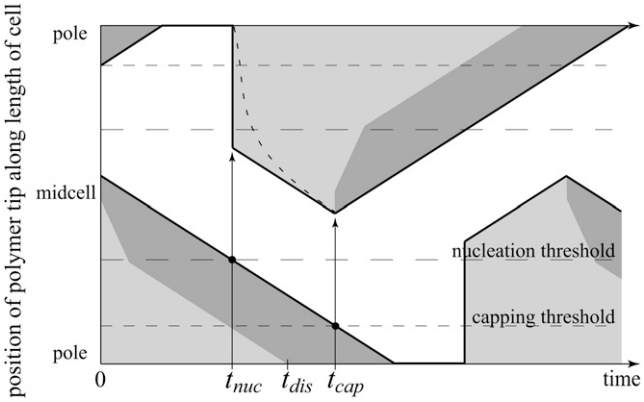

FIGURE 4 Approximate solution in the limit of rapid polymer growth. The exact solution differs only in the growth phase through which linear growth is replaced by an exponential approach to linear growth (*dashed curve*). The polymer at the lower pole is capped at $t = 0$ and is only seen disassembling under the influence of the E-ring (*dark shading*). The value t_{nuc} denotes the time at which the length of the lower polymer drops below the nucleation threshold (*long dashes*), meaning that the cytosolic MinD concentration is sufficient to nucleate the upper polymer. The value t_{dis} is the time at which the lower E-ring begins net disassembly. The value t_{cap} is the time at which the tip of the lower polymer crosses the capping threshold meaning the cytosolic MinE concentration is high enough to form an E-ring on the upper polymer. This process repeats with a period $T = 2t_{cap}$. Light shading represents MinD polymer without MinE and hence the region in which Z-ring formation is inhibited.

Cooperative nucleation and dimer-driven E-ring formation generate robust MinDE oscillations in wild-type cells

The stochastic-transition version of the model was implemented numerically to test the robustness of the model with respect to stochasticity and cooperativity. In the deterministic implementation, exaggerated cooperativity (i.e., sharp thresholds) lead to guaranteed oscillations—to what extent is cooperativity required? In the stochastic implementation, the probabilities of nucleation and capping were taken to be proportional to either the concentration of MinD and MinE, respectively (no cooperativity) or the cube of these concentrations (cooperativity).

In the latter case, oscillations persist in a manner quite similar to the deterministic case; compare the traces generated by simulating the stochastic model (Fig. 5 *A*) with the analytical solution to the deterministic model (Fig. 4). A visualization of one half-oscillation is provided in Fig. 5 *B* to illustrate the solution.

Interestingly, a nonlinear nucleation probability is not essential to having an alternating solution. When the probability of nucleation is taken to be a linear function of MinD concentration instead of a cubic function, MinD alternation stills occurs provided the nucleation rate is sufficiently high. However, the fidelity of polymers alternating between the poles is not as high in this case. For the nonlinear case, in a simulation lasting 1600 s, there were five skipped beats (i.e., a polymer appearing twice in immediate succession on the same pole) out of 118 nucleation events whereas in the linear case, there were 23 skipped beats out of 133 nucleation events. Note that on its own, this observation suggests that either a dedicated nucleation site or a critical nucleation phenomenon on the polar membrane (as described by the dimer-cycling equations) are both possible modes of polymer nucleation. However, it is difficult to reconcile a dedicated nucleation site with the *minE*$^-$ phenotype without additional assumptions about the influence of MinE on the nucleation site. We therefore consider the nonlinear case as the more viable option, since there is currently no evidence for a dedicated nucleation site.

Similar behavior is seen when the E-ring formation probability is taken to be a linear function of monomer concentration. In this case, oscillations were almost as consistent as for the nonlinear case (eight skipped beats out of 113 nucleation events in 1600 s). However, there was a marked increase in the variability in the time between the onset of E-ring disassembly on one MinD polymer and the moment of E-ring initiation on the nascent distal MinD polymer. This interval of time was measured to be 7.1 $\pm$ 4.3 s for the cubic

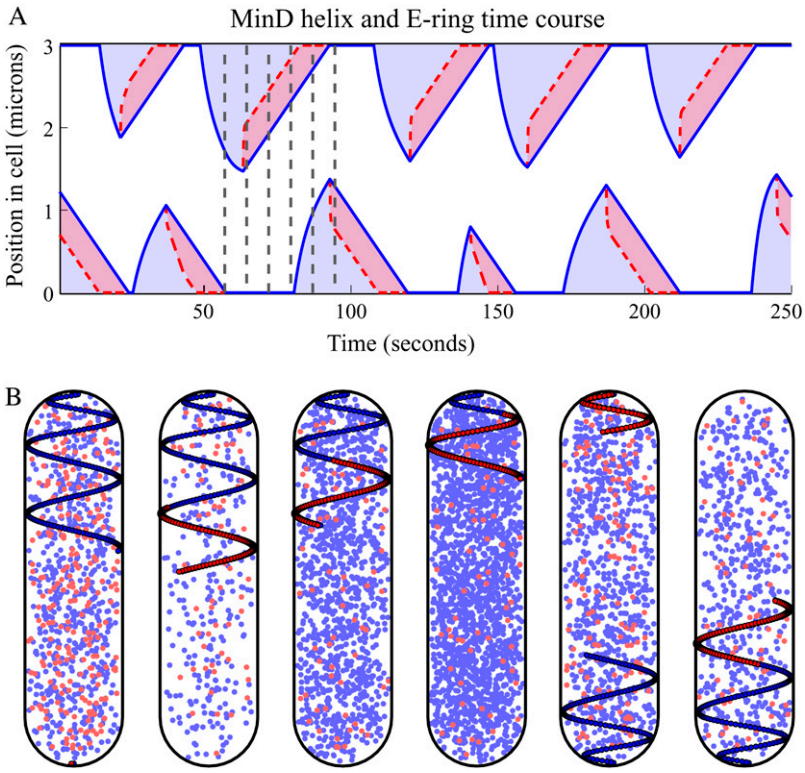

FIGURE 5 Numerical solution to stochastic implementation. (*A*) A set of traces from one run of the stochastic simulation. Blue curves represent MinD polymers tips; blue shading represents MinD polymers; red dashed curves denote the growing end of the E-rings; red shading represents E-rings. (*B*) A sequence of images showing approximately one half-period, generated from the traces in panel *A*. Each frame corresponds to a dashed line in panel *A* (from 57 to 94.5 in 7.5-s intervals). MinD polymer (*blue circles*, *outlined*), MinE ring (*red*, *outlined*), cytosolic MinD (*blue*, *no outline*), cytosolic MinE (*red*, *no outline*). For clarity, only half of the cytosolic MinD monomers, all cytosolic MinE dimers (but no monomers) and one out of every eight monomers in polymer form are shown. Note that in the model, polymer lengths and diffusively well-mixed cytosolic concentrations are tracked as scalar quantities; for visualization only, spatial distribution in the cytosol is by uniform random placement and the helical shape is prescribed (consistent with measurements from the images of (24)). Frame 1: A preexisting polymer is almost entirely disassembled (*bottom*). A new polymer (*top*) is growing. Note that cytosolic MinE dimer concentration is high, and as a result E-ring formation will occur soon on the growing polymer. Frame 2: An E-ring has formed; MinE dimer concentration is low and remains low until Frame 5; E-ring treadmilling is driven by monomer addition. Cytosolic MinD concentration is also low. Frame 3: Cytosolic MinD concentration rises as the upper polymer disassembles. Frame 4: The same trend continues. Frame 5: A MinD polymer has formed at the bottom and cytosolic MinE dimer concentration has begun to rise. Frame 6: Cytosolic MinE concentration has risen sufficiently to allow an E-ring to form on the lower polymer (equivalent to Frame 2, one half-period later).

function case and 7.1 ± 7.0 s for the linear case. The extreme variability observed was anticipated but it was expected to lead to a complete failure in the polar alternation of polymerization. Interestingly, this was not the case.

In this study, we consider only whether the polymer undergoes a relatively consistent alternation from pole to pole. If a more careful analysis were carried out—for example checking for the presence of temporal gaps in the polar localization of MinD long enough to allow FtsZ to form a Z-ring at a MinD-less pole—these linear cases would likely generate higher rates of minicelling than seen in wild-type cells.

A qualitative sense of the difference between the linear and nonlinear regimes can be gained from Fig. 6. Note that parameter values in the linear cases are identical to those in the nonlinear case except that, for linear nucleation of MinD, the nucleation rate is taken to be an order of magnitude larger than in the nonlinear case and for linear E-ring formation, the formation rate is taken to be an order of magnitude lower. As well, for the linear E-ring case the cytosolic MinE pool is assumed to be entirely in monomer form, consistent with the absence of cooperativity in the form of dimerization.

Across all model variations simulated, including all four permutations of linear and nonlinear MinD nucleation and E-ring formation, the measured statistics other than those already mentioned were approximately the same. For example, the oscillation period was, on average, 50 s in all cases. Also, the maximal fraction of the cell covered by polymer was ≈34% ± 13%, which is in good agreement with observations (24).

Mutants

Reverse genetics offer a powerful tool for exploring the different roles played by distinct domains of a single protein. Such studies also provide an effective way of testing a model. With the Min proteins, much work has focused on overexpression, deletion, truncation, and point mutations of MinE. In this section, we describe the widespread agreement between the mutant phenotypes and the corresponding predictions that arise from the proposed model.

Cells lacking MinE (*minE*$^-$) show a uniform membrane localization of MinD

In the absence of MinE, MinD appears to associate with the membrane but fails to nucleate polymers (8,56). This is counterintuitive, as MinE is known to inhibit the association of MinD with the membrane but it is also apparently necessary for polymerization. The paradox is easily resolved by the dimer-cycling model. In the model, without MinE, the polar and nonpolar membrane concentrations of MinD are essentially the same and relatively low in comparison with polar concentrations in wild-type cells, bringing the nucleation probability below the critical level. In different contexts, this

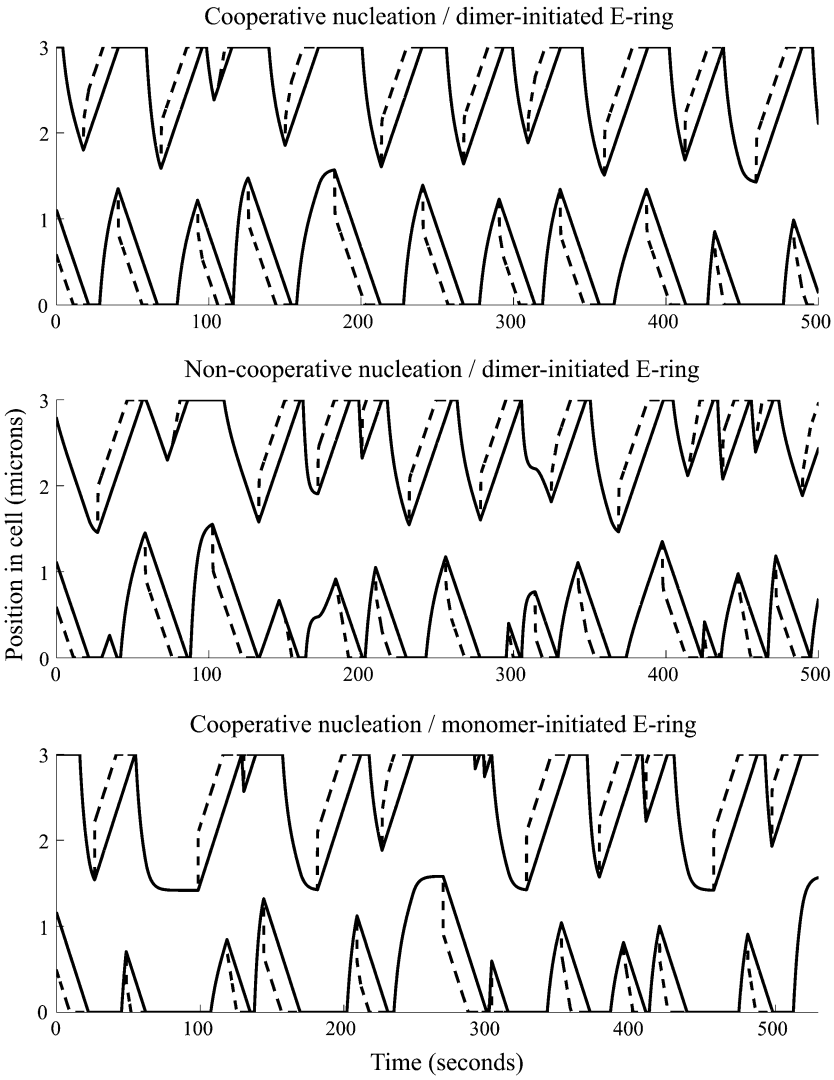

FIGURE 6 Polymerization dynamics in three different types of theoretical cells. One cell with nonlinear nucleation of MinD and nonlinear capping by MinE (*top*), one with linear nucleation of MinD and nonlinear capping by MinE (*middle*), and one with nonlinear nucleation of MinD and linear capping by MinE (*bottom*). Notice the loss of regularity in the lower two panels.

polymerless phenotype causes either minicelling (8,56) or a complete block of division (5,56). We infer that the difference between these two cases depends on the expression level of MinD. At low concentrations, membrane-bound dimers are unable to recruit sufficient MinC to suppress Z-ring formation whereas, at higher concentrations, enough MinC is recruited and is recruited uniformly across the cell leading to suppression of division everywhere. The necessary condition for this explanation, which provides a testable prediction, is that for increasing membrane-bound MinD dimer concentration, one should see no FtsZ suppression at low concentrations, followed by global suppression, followed by polymer formation at high concentrations.

Overexpression of *minE* and *minD*

Overexpression studies have demonstrated that the total concentrations of both MinD and MinE have an influence on phenotype and, in particular, when MinD still undergoes wild-type oscillations, on the period of the oscillation. Using the available data, estimation of parameter values is possible. We demonstrate that by fitting only two unknown parameters, the model can be made consistent with a range of phenotypes and captures quantitative trends in the experimental data.

We focus on a subset of the observations of Raskin and deBoer (6) for which the oscillation condition and the expression for oscillation period T are valid (see MinDE Oscillations). Each of the following described experiments was carried out by introducing a λ-phage to express the desired protein(s). We assume that for each protein, expression levels are the same but, as with the endogenous proteins, other factors lead to a 4:3 ratio in the concentration of MinD to MinE (24).

Wild-type cells were found to oscillate with an average period of 38 s. Overexpression of *minD* in a wild-type background showed wild-type division patterns, but it was found that the MinD oscillations have a period of 96 s, significantly

longer than unperturbed cells. Interestingly, simultaneous overexpression of both *minD* and *minE* in a wild-type background returned the oscillations to normal periodicity (40 s) (8). Expression of both *minD* and *minE* in a Δ*minCDE* mutant failed to rescue the minicelling seen in Δ*minCDE* cells but oscillations of a period similar to wild-type cells were reported (8). In later experiments, it was found that higher expression levels of *minD* and *minE* were able to restore the wild-type phenotype, including the oscillation period in the Δ*minCDE* mutant (13).

These results can be explained by the model in a quantitative manner and in doing so, provide an estimate of the plasmid expression level λ and E-ring threshold E_{thresh}. Equating the experimental values for oscillation periods with the expression for the period derived from the deterministic model, replacing D_{tot} and E_{tot} by $D_{\text{tot}} + \lambda$ or λ and $E_{\text{tot}} + 3/4\lambda$ or $3/4\lambda$ when appropriate depending on the experiment in question, gives a system of four overdetermined equations in terms of the unknown parameters E_{thresh} and λ. A least-squares fit provides values of $E_{\text{thresh}} = 2.5\ \mu$M and $\lambda = 3.3\ \mu$M such that the predicted periods are roughly consistent with those reported in Raskin and de Boer (8) (see Table 3). In addition, the fact that $3/4\lambda \sim E_{\text{thresh}}$ means that when *minDE* is expressed in a Δ*minCDE* cell at a level λ, there is just barely enough MinE to initiate an E-ring. Thus, under stochastic variations, E-rings might occasionally fail to form, thereby delaying the oscillations and allowing for polar Z-ring formation. This offers a possible (and testable) explanation for the observed minicell phenotype. At higher MinE expression levels, E-ring formation would not be a problem, which is consistent with the later observation that higher expression levels rescued the minicell phenotype. The predicted value of λ is therefore considered to be and is henceforth referred to as ''low,'' relative to wild-type levels.

The analytical solution also allows for the estimation of the maximum percentage coverage of the cell length by the MinD polymer (included in Table 3 and visible in Fig. 4 as the maximum height at $t = 0$ and $t = t_{\text{cap}}$) and the length of time during which different cell locations are exposed to Z-ring formation (the width of the *unshaded zones* at different heights in Fig. 4), both useful in understanding two other experiments. Intermediate levels of *minD* overexpression in a wild-type background caused minicelling and at yet higher levels, complete block was seen (8). Notice that even at low levels of *minD* overexpression, the MinD helix is predicted to cover 78% of the cell when at its maximum length. This means that the midcell region is exposed to FtsZ for a brief portion of the oscillation, ~25 s for the parameters in Table 2, whereas the poles are exposed for only ~15 s. At intermediate levels of exogenous expression ($\lambda \sim 5.3\ \mu$M instead of $3.3\ \mu$M), the window of opportunity for Z-ring formation closes down completely at midcell. However, there is ~20 s of exposure at the poles coincident with a lengthening of the oscillation period (150 s) so minicelling is a more likely option. For higher expression levels (~$7.3\ \mu$M), a polymer originating at either pole reaches all the way across to the opposite pole (predicted maximal coverage of 110%), thereby shutting down all options for Z-ring formation, which explains the observed complete division block. This method of estimating the influence of overexpression on Z-ring formation provides a powerful tool for quantitatively analyzing experiments on FtsZ-GFP expressing *E. coli* in the presence of Min overexpression.

Another related phenotype is the overexpression of *minE* in a wild-type background, which causes minicelling (5). This can be explained by the oscillation condition in that, if the right-hand side of the inequality is increased by >0.5–2 μM (depending on the exact value of D_{thresh}) above wild-type values, the condition is no longer satisfied (hence minicelling).

TABLE 3 Results of fitting parameter values to data

Genotype	Oscillation period	Maximum coverage
Wild-type	45 s (38 s)	40%
minD overexpression	94 s (96 s)	78%
minDE overexpression	20 s (34 s)	50%
minDE expression in Δ*minCDE*	50 s (40 s)	38%

Fitted oscillation periods and resulting maximal MinD coverage are given for each expression experiment. Experimentally measured values (8) are in parentheses. These data were fitted by a least-squares method generating predictions for expression level, $\lambda = 3.3\ \mu$M, and E-ring-formation threshold, $E_{\text{thresh}} = 2.5\ \mu$M. This value of λ is low relative to wild-type levels.

Minicelling with 1), a truncated form of MinE ($MinE^{1-22}$), and 2), a two-point-mutation, $MinE^{D45A/V49A}$

These two cases are similar in the sense that both are characterized by having an anti-MinD domain that is incapable of being correctly localized to a MinD polymer tip due to lack of TS residues (see Fig. 1 *A*). In the case of $MinE^{1-22}$, the entire protein consists only of the anti-MinD domain and is missing the TS residues, which are essential for MinE to properly control MinD localization (47). The other, $MinE^{D45A/V49A}$, has had the TS residues mutated and has been shown to be incapable of forming E-rings (24). Due to the predicted similarity between these two mutants, only $MinE^{D45A/V49A}$, for which MinD-GFP fusions have been made and studied (24), is described here.

The *minE*$^{D45A/V49A}$ phenotype at the level of fluorescence observations was described in detail by Shih et al. (24). In contrast with the complete absence of MinE, cells with MinE replaced by $MinE^{D45A/V49A}$ are still capable of MinD polymerization. In the context of our model, this means that the hydrolysis-inducing domain of $MinE^{D45A/V49A}$ is still capable of clearing MinD dimers from the nonpolar regions of the membrane even without functional TS residues and so the mechanism for polar nucleation remains intact. Note that this is the only explicit role for $MinE^{D45A/V49A}$ in the proposed

model; hydrolysis in the polymer is assumed to be predominantly spontaneous due to the absence of the otherwise more effective E-ring.

The $MinE^{D45A/V49A}$ mutant was found to differ from wild-type MinE in several ways other than the lack of E-rings. MinD helices extended further than in wild-type cells, often reaching beyond midcell. MinD disassembly occurred but in a disrupted manner, sometimes stuttering with an assembly phase interspersed with disassembly and often reaching all the way to the opposite pole with subsequent disassembly starting from either pole after a ''highly variable time.'' In general, disassembly was significantly slower than in wild-type cells with typical timescale for disassembly in the range of 5–15 min (24). In addition to these fluorescence observations, minicelling was observed.

Recall that MinD is capable of hydrolysis in the absence of MinE at a reduced rate (11). In addition to this, we incorporate the following assumptions into a model of this mutant. First, we assume that disassembly of the MinD polymer is slowed in the polar regions. Furthermore, we assume that once a MinD polymer assembles, individual subunits hydrolyze their ATP at an exponentially distributed time after incorporation into the polymer. Finally, we assume that when MinD-ATP is at the exposed tip of the polymer, subunits can add, but when MinD-ADP is at the tip, they either do not add or else only do so at a much reduced rate. This model is similar to those proposed for the dynamic instability of microtubules dynamics (57) and ParM (58). We implemented this model computationally using a Gillespie algorithm (59), treating monomer addition to an ATP-tipped polymer, hydrolysis, monomer disassembly from an ADP-tipped polymer, ATP-ADP exchange in the cytosol, and polymer nucleation as stochastic events with probabilities corresponding to the mean rates used in the deterministic model described above. MinE-independent hydrolysis was taken to be a factor of 10 slower than MinE-dependent disassembly rate listed in Table 2.

As shown in Fig. 7, simulations of this mutant model demonstrate behavior similar to that seen experimentally. Occasional stuttering (highlighted by *solid circles*) is seen due to incomplete hydrolysis within the polymer lattice even once monomers at the polymer tip have hydrolyzed, allowing partial disassembly followed by rescue (to use terminology adopted from microtubule dynamic instability). The polymer generally grew longer than normal, not being stopped by E-ring formation. Upon reaching the distal pole, disassembly would begin after a variable period of time sometimes from the distal pole (alternating black arrows), sometimes from the nucleating pole (*nonalternating arrows*). Subsequent nucleation (*solid arrows*) always occurred at the same pole as disassembly. In the simulations, the timescale for disassembly was set by the strength of the polar stabilization; in the example shown, it was roughly a few hundred seconds.

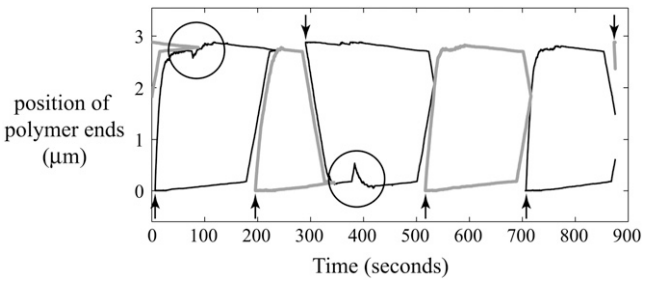

FIGURE 7 The $MinE^{D45A/V49A}$ mutant model. Each pair of solid (*shaded*) curves correspond to the positions of the ends of a single polymer through time. Arrows denote nucleation. Nucleation alternated from one pole to the other provided the preceding polymer began disassembly at the nonnucleating pole. Occasionally, disassembly began at the same pole as nucleation. Circles highlight stuttering.

Wild-type cells with expression of a $MinE^{22–88}$ fragment

Expression of the 66 C-terminus amino acids of MinE in an otherwise wild-type cell at levels comparable to the wild-type MinE protein results in a minicell phenotype (36). In deciphering this phenotype, it was shown that $MinE^{22–88}$ can form homodimers as well as heterodimers with MinE (36). What does this mean in the context of our polymer model? Assuming dimerization occurs at random, ~25% of dimers would be MinE homodimers, 50% would be heterodimers and 25% would be $MinE^{22–88}$ homodimers. With all three types of dimers having an intact TS domain, an E-ring initiated by one of the first two types but composed of all three should form. With twice as many total dimers available, the E-ring would be longer than usual (keeping total cytosolic dimer concentration at E_{crit}) and should therefore begin to disassemble earlier than usual, as with overexpression of wild-type MinE. However, despite the possibility of early E-ring formation, during E-ring treadmilling one out of every two dimers would be incapable of inducing MinD hydrolysis whether due to a heterodimer with its sole anti-MinD domain facing away from the tip or due to a $MinE^{22–88}$ homodimer with no anti-MinD domain at all. This would cause a stuttering in the disassembly, allowing cytosolic MinD to attach at the tip and possibly destabilizing the E-ring. Without E-ring processivity, the MinD-less pole would be left for extended periods of time unprotected from Z-ring formation, thereby allowing minicelling.

When $MinE^{22–88}$ was expressed at much higher levels, so high that essentially no wild-type homodimers form (as determined by immunoblotting), a complete block of division was seen (36). An independent study showed that mutations to MinD's α-7 α-helix allows MinC to outcompete MinE, which is not its normal behavior (50). A mutation to α-7 on MinD is in some sense equivalent to a loss of the anti-MinD domain on MinE, because these domains are known to interact (51). Provided MinC can outcompete the heterodimers which would theoretically have an affinity for MinD somewhere between that of wild-type and mutant homodimers, this competition would severely limit the dimer cycling

required to concentrate the MinD dimers at the poles and simultaneously lead to a complete block of division. This problem would not arise at the lower expression level because of the presence of wild-type homodimers.

Interestingly, expressing a slightly shorter protein, $MinE^{36–88}$, in wild-type cells also causes minicelling; however, this phenotype persists over a wide range of concentrations and does not transition to a division-failure phenotype at high concentrations as seen with $MinE^{22–88}$. The difference between these two truncations is that $MinE^{36–88}$ monomers are incapable of forming heterodimers with wild-type monomers and presumably homodimers with itself (36). This truncation is apparently missing only part of the dimerization domain, as it still retains a pair of β-sheet strands and a coiled coil involved in dimerization (49). The fact that the debilitated protein is able to cause minicelling might be explained by the fact that although monomers are unable to initiate an E-ring, they can still elongate an existing E-ring. Even if $MinE^{36–88}$ is incapable of dimerizing in the cytosol, it might still be able to bind as a monomer to the E-ring and subsequently dimerize under the stabilizing influence of the MinD polymer and existing E-ring. Once incorporated into the E-ring, the truncated protein would have the same processivity-reducing influence on MinD helix disassembly as described for the longer fragment. The transition to complete division block at higher expression levels would not occur here, because the only dimers to form would be wild-type homodimers and these would be sufficient to outcompete MinC for membrane-bound MinD dimers.

DISCUSSION

In this article, we have put forward several new ideas, wrapped in the framework of a quantitative model, to link a broad range of experimental results across several scales from protein structure to cellular phenotype.

The combination of global membrane attachment by MinD-ATP and a polar bias in the induction of MinD's ATPase activity by MinE provide an explanation for the observed polar bias and cooperativity of MinD polymer nucleation. The details of this mechanism allow for consistency with the observed *minE*$^-$. We propose that lower MinE activity at the poles is due to a lack of strain in the MinD dimer, but this is only one possibility, which illustrates a general principle. Independent of the details of the mechanism, the general principle simultaneously accounts for nucleation at the poles in wild-type cells and a lack of nucleation in the *minE*$^-$ mutant.

It is worth noting that global attachment is an explicit assumption in all SPF models, but the effect of our assumed spatially graded hydrolysis-induction by MinE is accomplished in other models either through the dynamic formation of concentration gradients (17) or through the assumption of an aggregation current (16,20). Other desirable features of the polymer model presented here, for example restriction of subunit turnover to the polymer tip, rule out the adoption of assumptions that allow SPF in other models (17). The aggregation-current models (16,20) seem to have some polymerlike features but notably fail to correctly predict MinE distribution, in particular the MinE ring, which arises more naturally in the explicit polymer description presented here.

In fact, the details of MinE protein structure strongly motivate the major assumptions underlying this protein's roles in division site selection. The N-terminus anti-MinD domain plays the dual role of hydrolysis induction and suppression of MinD polymer growth through steric exclusion at the polymer tip. The TS residues (45 and 49) allow for the formation of the E-ring, which imparts processivity to the MinE-induced disassembly and delays formation of the next E-ring by cytosolic depletion of MinE. Finally, concentration-dependent dimerization in the cytosol via the C-terminus α-helix and β-sheet is also necessary to properly control the timing of E-ring formation. Together, these component parts impose on the MinD polymer two distinct states, an assembly state and a disassembly state, through which correct division site selection is rapidly accomplished, as discussed in more detail below. The large set of mutant studies provide a clear means of testing out the details of these proposed roles; the mathematical model successfully provides a connection between protein function at the molecular scale and the emergent phenotypes at the cellular scale in all cases discussed. In addition, many of these explanations provide hypotheses that can be tested by fluorescence microscopy.

Dynamic instability of MinD provides a sufficiently rapid means of suppressing polar division

Dynamic instability of microtubules has been described as a means by which a cell can rapidly search through intracellular space. Theoretical estimates of capture times for chromosomes during prometaphase in eukaryotic cells showed dynamic instability to be more efficient than reversible polymerization, which proceeds by interspersed addition and removal of monomers (33). For *E. coli*, the difference between these two modes of polymer dynamics is clearly demonstrated by the $MinE^{D45A/V49A}$ mutant. In wild-type cells, MinD nucleates and grows rapidly until MinE caps it, switching it from a growing state to a shrinking state, analogous to microtubule catastrophe. When E-ring formation is prohibited in the $MinE^{D45A/V49A}$ mutant, distinct growth and shrinking states are suppressed, and are replaced by less reliable spontaneous hydrolysis, which leads to longer polymers as well as stuttering in the disassembly process. Although this mutant polymerization regime is not reversible polymerization (interspersed assembly and disassembly), it demonstrates dynamic instability that is characterized by a slower catastrophe rate and more rapid rescue rate than the wild-type cells, which undergo catastrophe early enough to stop at midcell and are never rescued. In this sense, they are closer to the reversible polymerization regime in terms of the delayed nature of

polymer turnover. The corresponding change in timescales of complete assembly and disassembly leaves enough time for the formation of a polar Z-ring thereby causing minicelling. Restating these observations in terms of the regime seen in wild-type cells, the E-ring-dependent dynamic instability of the MinD polymers accelerates the cycle of polar Z-ring suppression, thereby preventing minicelling. This description reiterates the fact that dynamic instability is not an isolated trick discovered by tubulin but is a general principle employed by nonhomologous systems to carry out time-sensitive tasks, a feature also recently observed in the bacterial actin homolog ParM (58). Interestingly, the MinD system admits oscillations in polymer length not seen in small collections of microtubules but have been observed in in vitro bulk experiments (60,61) and studied theoretically (62,63).

Nonlinearity provides robustness in the face of stochasticity

Cooperativity has been reported in both MinD polymer formation and MinE-induced hydrolysis (11,25,32). The exact role played by cooperativity in vivo is not clear. In comparison with the deterministic model, when stochasticity of MinD polymer nucleation and E-ring formation are introduced, they perturb the regularity of the oscillations. However, the perturbation is not severe provided nucleation probabilities are nonlinear functions of protein concentrations. The robustness of the oscillations can thus be interpreted to be at least in part due to cooperative features of multistranded polymer nucleation and capping. This relationship between stochasticity and cooperativity has been demonstrated previously in other biological systems (for example, in the regulation of the PER protein in circadian rhythms (64)).

Experiments and predictions

The model provides predictions for phenotypes that have not been previously observed or have not been subject to quantification and also suggests several experiments that would be useful in discriminating between various models. We describe some of these here.

With the exception of the model of Drew et al. (26) and the model presented here, there is apparent agreement in the mathematical modeling literature that MinDE oscillations arise spontaneously from the activity of MinD and MinE and do not depend on anatomical cues upstream of these proteins. To date, there is no compelling direct evidence to support or refute this hypothesis. It was observed early on that filamentous mutants, which grow significantly longer than wild-type cells, show MinD oscillations with an increasing number of stripes as they lengthen (8). This observation was the original motivation for the invocation of a Turing-like mechanism to explain the dynamics and indicates that MinD localization is not directly linked to the poles. However, Mileykoskaya et al. (28) demonstrated that the lipid domains they observed in wild-type cells also appeared in filamentous mutants with additional localization to the midcell region, in a pattern complementary to the localization of the DNA and similar to the pattern of MinD nucleation in the filamentous stripes. This suggests that a lipid domain gradually develops at midcell as the replicated chromosomes are segregated. Although a causal link between nucleoid and lipid domain localization is called into question by observations of anucleate cells (65), other mechanisms for lipid domain formation are possible. In wild-type cells, provided the lipid domain maturation with respect to MinD recruitment is slower than Z-ring formation, such a domain might not recruit MinD until after division when it finds itself at the nascent poles of the daughter cells. In a filamentous cell lacking these new poles, this developing lipid domain could lead to the late appearance of a third MinD nucleation zone. Simultaneous labeling of cardiolipin and MinD in a filamentous mutant would allow for a distinction between the two hypotheses—does the appearance of a midcell MinD zone correlate with cell length or with the appearance of the midcell lipid domain?

Below a critical concentration, MinD fails to tubulate vesicles in the in vitro assays (11). At these low concentrations, MinD is likely attached to the vesicles in unpolymerized dimer form. Can MinE still induce hydrolysis under these conditions? If so, what is the ratio of MinE-induced hydrolysis to background hydrolysis at MinD concentrations that are below the tubulation threshold? Are these hydrolysis rates sensitive to the vesicle membrane tension? Is the tubulation threshold sensitive to membrane tension?

The α-5 and α-6 domains of MinD are α-helices that are exposed on the face of membrane-bound MinD (i.e., directly opposite its membrane-binding domain). They are also situated beside α-7, the domain thought to bind to MinE's anti-MinD domain (51). These domains are the most likely candidates for interaction with the TS residues of MinE. Can $MinE^{32-88}$, which lacks the anti-MinD domain, bind to MinD? If so, is the binding sensitive to mutation of the TS residues or mutations in α-5 and α-6? Is it sensitive to mutations in MinD's α-7?

In cells expressing the truncated protein $MinE^{1-22}$, does MinD behave similarly to what is seen in cells expressing $MinE^{D45A/V49A}$? In either of these cells, does quantitative measurement of MinD helix dynamics agree with the proposed stochastic hydrolysis model? Similarly, fluorescence microscopy of GFP-tagged MinD in the $MinE^{22-88}$ and $MinE^{36-88}$ mutants would allow simple tests of the proposed explanations for these mutants.

We hypothesize here that MinE's anti-MinD domain is the analog of the α-helix that is present on the analogous ATPase NifH but missing from MinD (39). Does truncation or point-mutation of the C terminus α-helix from NifH eliminate its capacity to hydrolyze ATP? Does reintroduction of the helix to the truncated NifH rescue hydrolysis, as seems to be the case for MinD when $MinE^{1-22}$ is reintroduced (47,48)?

The reason suggested by our model for the failure of MinD to polymerize in the absence of MinE is that MinE selectively removes MinD from the nonpolar membrane, thus allowing the polar concentration to rise above nucleation threshold. A resulting prediction is that sufficient overexpression of MinD in the *minE* mutant should cause nucleation at random on the cell membrane, not unlike the phosphatidylethanolamine mutant phenotype (29).

Quantitative measurements of the position of Z-ring formation along the axis of the cell in the presence of MinD and/or MinE overexpression can be compared to predicted probability densities generated by a technique similar to that described in Overexpression of *minE* and *minD* in Results. This would provide both a means of testing the model as well as a quantitative in vivo understanding of the influence of the Min system on Z-ring positioning.

APPENDIX

Strain in membrane-bound MinD dimers

In tubulating vesicles, MinD does work—the energy for which ultimately derives from the high energy ATP-bound state of MinD and, we assume, is temporarily stored in strain energy in the membrane-bound dimer. This strain energy is used to overcome the activation energy for hydrolysis and so when strain is not maintained, the hydrolysis rate is slowed. By calculating the energy per monomer required to tubulate a vesicle of a particular size, we get a lower bound on the energy that can be stored in a strained MinD dimer.

Consider a vesicle of radius $R_0 = 400$ nm being deformed as shown in Fig. 2. When a tube of length $l = 400$ nm and radius $r = 25$ nm is extracted from the vesicle, the osmotic pressure and the membrane surface tension equilibrate determining the overall volume contained within. The equation for mechanical equilibrium of this partially tubulated vesicle is

$$2K_s(A - A_0)/(RA_0) = p_0(V_0/V - 1),$$

where $A = 4\pi R^2 + 2\pi rl$ is the total surface area of the deformed vesicle, A_0 is the undeformed surface area, $V = 4/3\pi R^3 + \pi r^2 l$ is the total volume of the deformed vesicle, V_0 is the undeformed volume, $p_0 = 9.4 \times 10^7\ k_BT/\mu m^3$ is the osmotic pressure of the buffer (estimated from Methods in (11)), $K_s = 4 \cdot 10^7\ k_BT/\mu m^3$ is the membrane stretching modulus (66), and R is the radius to which the spherical portion of the vesicle equilibrates. Given any value of l, a value of R can be found and from that, the energy stored in stretching the membrane can be calculated: $E = K_s/2\,(A - A_0)^2/A_0$. The difference in energy between a vesicle with a tube of length $l = 400$ nm and $l = 406$ nm, which corresponds to the addition to the tube of a ring of 25 dimers, is 181 k_BT or 7.2 k_BT per dimer.

Note that it is possible that the membrane is ruptured during the process (see (11)). However a 400-nm-long tube pulled from a 400-nm-radius vesicle represents a percentage stretching of ~1.2%, which is below the range of membrane rupturing (67), so rupture would not occur within the range relevant to the calculation presented here.

MinD forms a double-stranded polymer

To address the question of the ultrastructure of the MinD polymer, we calculate the fraction of the cell that can be wrapped by a MinD helix as a function of the presumed structure of the polymer given available estimates from the literature for the relevant biophysical parameters. The calculation indicates that a double-stranded helix is the most likely arrangement for a MinD polymer. It also suggests that a single MinD helix extends from pole to midcell.

The maximum possible length of a polymer is $l_{max} = N_D\Delta$, where N_D is the total number of monomers available, Δ is the diameter of a monomer, and n is the number of strands in the polymer. The MinD polymer forms a helix with an angle of $\sim\theta = 80°$ relative to the long axis of the cell (measured from images in (9); see Parameter Estimation, below) so the length of the polymer projected onto that axis of the cell is $L_p = l_{max}\cos\theta$. As a fraction of the length of the cell (L), the projected length can be expressed as $f = L_p/L = 600c\pi r^2\delta\cos(\theta)/n$, where c is the total concentration of MinD in μM, and r is the radius of the cylindrical cell. Provided the concentration of MinD is regulated so as not to change as a cell grows, this maximal-length covering-fraction is independent of cell length. Based on estimates extracted from the literature, $c \sim 4\ \mu$M (9,35), $r \sim 0.35$–$0.5\ \mu$m (6), $\Delta \sim 5$ nm (25), and $\theta \sim 80°$ (9), it is clear that for $n = 2$ the maximal covering-fraction is reasonable ($f = 0.4 - 0.8$) and for $n = 3$, a maximum length polymer would barely be capable of reaching midcell ($f = 0.25$–0.55). Based on the $minE^{D45A/V49A}$ mutant which demonstrates that MinD can reach from pole to pole, $n = 3$ is less likely than $n = 2$. For $n = 4$ (or greater), there is insufficient MinD to cover >40% of the cell's length. Due to the general prediction of short lengths for single-stranded polymers (15), $n = 1$ is also unlikely, requiring an unrealistic polymer-tip dissociation constant for MinD-ATP of $10^{-5}\ \mu$M to achieve sufficient lengths. Finally, a two-stranded model is the most consistent with the dimer structure of MinD (38) and with the electron microscopy observations of Suefuji et al. (25).

Solution to model equations

Suppose the left MinD polymer is of length l_0 at $t = 0$ with an E-ring of length l_{E_0}, and no polymer is present at the right pole. The length as a function of time, until complete disassembly, is

$$l(t) = -\beta t + l_0,$$

where $\beta = \delta k_{dep}$. A polymer nucleates at the right pole at $t = t_{nuc}$, where $D(t_{nuc}) \equiv D_{tot} - \gamma l(t_{nuc}) = D_{thresh}$ and $\gamma = 1/(V\delta)$. Thus, the nucleation time is

$$t_{nuc} = l_0/\beta - (D_{tot} - D_{thresh})/(\beta\gamma).$$

Assuming $k_{poly}D_{tot} \gg k_{dep}$, the right polymer quickly equilibrates to length

$$r(t) = D_{tot}/\gamma + \beta t - l_0,$$

an expression valid from t_{nuc} until the polymer is capped. The system can still be solved without this scaling assumption but this assumption does not introduce large errors and so reduces the complexity of the solution without great loss. Capping on the right occurs when the left E-ring disassembles to the point that the cytosolic concentration rises to E_{thresh}. Disassembly begins when $l(t) = l_{E_0}$, from which point the length of the E-ring is the same as the length of the MinD polymer. The E-threshold is reached when $E(t_{cap}) \equiv E_{tot} - \gamma l(t_{cap}) = E_{thresh}$, which occurs at

$$t_{cap} = l_0/\beta - (E_{tot} - E_{thresh})/(\beta\gamma).$$

The length of the right polymer upon getting capped is

$$r(t_{cap}) = (D_{tot} - (E_{tot} - E_{thresh}))/\gamma.$$

Assigning this value to the initial length of the left polymer as well means that t_{cap} is also the half-period of the oscillation. Thus, the period of the oscillation is given by

$$T = 2\,(D_{tot} - 2(E_{tot} - E_{thresh}))/(\beta\gamma).$$

The oscillatory solution exists provided a nucleated polymer is not capped immediately upon forming: $t_{nuc} < t_{cap}$. This reduces to the condition

$$D_{tot} - D_{thresh} > E_{tot} - E_{thresh}.$$

Parameter estimation

Parameter values in Table 2 with sources stated as a citation only were found explicitly in the cited reference. ''Estimated from'' indicates that values were implicit and some calculations and/or measurements from images were required. Values for k_{dep}, k_{poly}, and k^{E}_{poly} were estimated from sequences of fluorescence images showing the temporal progression of the oscillations. k_{poly} and k^{E}_{poly} were taken simply so as to ensure polymerization was as fast or faster than disassembly; that is, unless assembly is notably slower than disassembly, k_{dep} alone sets the timescale of the process. D_{tot} and E_{tot} were calculated from published estimates for the number of MinD and MinE monomers per cell (24,35) and an estimated average cell volume. The pitch of the MinD helix, θ, was estimated from fluorescence images in Shih et al. (9) by measuring and averaging cell aspect ratios and number of apparent wraps from several images. The estimate of $\theta = 80°$ was confirmed by generating arrays of point sources of light in helices at various angles as in Fig. 5 *B* and convolving them with a Gaussian PSF to get an artificial fluorescence image. Visual inspection ruled out angles $<\sim 77°$.

In the stochastic implementation with $\{n = 3, m = 3\}$, for the parameters k_{nuc} and k_{cap}, all values within the given range were tested and demonstrated oscillations. At the edges of the ranges, qualitative similarities to what is seen experimentally gradually break down, with delayed or overly rapid nucleation and/or E-ring formation as well as skipped beats occurring often. Values used for the trace in Fig. 5 were $k_{nuc} = 0.006\ \mu M^{-3}\ s^{-1}$ and $k_{cap} = 0.4\ \mu M^{-3}\ s^{-1}$.

Diffusion and ADP-ATP exchange are two processes that have been invoked as crucial elements in various models in the literature. Due to the estimated timescales associated with each of them, we have taken them to be in quasi-steady state. The cytosolic diffusion coefficient of both MinD and MinE has been taken to be $D = 2.5\ \mu m^2/s$ in previous models based on measurements for an unrelated protein in *E coli*. (68). Recent FCS measurements for MinD-GFP indicate that $D = 16\ \mu m^2/s$ (69). The time constant for the former value in a cell 2–3 μm in length is $L^2/(2D) \sim$ 1–2 s and 0.1–0.3 s for the more recent FCS-based estimate.

The timescale for ADP-ATP exchange is not known for MinD but previous models have assumed a value at ~1–2 s (17,21,22,30) and others have either implicitly or explicitly assumed it to be rapid relative to other processes (14–16,20,26). Given that the time from onset of disassembly at one pole to nucleation at the other pole is necessarily less than the time required for Z-ring formation (~30 s (70)) and requires at least one exchange per MinD monomer, the ADP-ATP exchange rate must be at least that fast. Provided the time constant for exchange is <10 s (roughly the minimum time between disassembly onset and nucleation), it would not influence the dynamics of our model significantly.

The authors acknowledge L. R. DeBella, L. Edelstein-Keshet, A. Mogilner, P. Borowski, and the anonymous reviewers for valuable feedback on the manuscript and P. Fletcher for help with generating figures.

E.N.C. is supported by funding from National Sciences and Engineering Research Council (Canada) and Mathematics of Information Technology and Complex Systems; B.D.L.M. was funded through the National Sciences and Engineering Research Council (Canada)-Undergraduate Student Research Awards summer program.

REFERENCES

1. Margolin, W. 2005. FtsZ and the division of prokaryotic cells and organelles. *Nat. Rev. Mol. Cell Biol.* 6:862–871.
2. Yu, X., and W. Margolin. 1999. FtsZ ring clusters in min and partition mutants: role of both the Min system and the nucleoid in regulating FtsZ ring localization. *Mol. Microbiol.* 32:315–326.
3. de Boer, P., R. Crossley, and L. Rothfield. 1992. Roles of MinC and MinD in the site-specific septation block mediated by the MinCDE system of *Escherichia coli*. *J. Bacteriol.* 174:63–70.
4. Hu, Z., A. Mukherjee, S. Pichoff, and J. Lutkenhaus. 1999. The MinC component of the division site selection system in *Escherichia coli* interacts with FtsZ to prevent polymerization. *Proc. Natl. Acad. Sci. USA.* 96:14819–14824.
5. de Boer, P., R. Crossley, and L. Rothfield. 1989. A division inhibitor and a topological specificity factor coded for by the minicell locus determine proper placement of the division septum in *E. coli*. *Cell.* 56:641–649.
6. Raskin, D., and P. de Boer. 1999. MinDE-dependent pole-to-pole oscillation of division inhibitor MinC in *Escherichia coli*. *J. Bacteriol.* 181:6419–6424.
7. Hu, Z., and J. Lutkenhaus. 2001. Topological regulation of cell division in *E. coli*. spatiotemporal oscillation of MinD requires stimulation of its ATPase by MinE and phospholipid. *Mol. Cell.* 7:1337–1343.
8. Raskin, D., and P. de Boer. 1999. Rapid pole-to-pole oscillation of a protein required for directing division to the middle of *Escherichia coli*. *Proc. Natl. Acad. Sci. USA.* 96:4971–4976.
9. Shih, Y., T. Le, and L. Rothfield. 2003. Division site selection in *Escherichia coli* involves dynamic redistribution of Min proteins within coiled structures that extend between the two cell poles. *Proc. Natl. Acad. Sci. USA.* 100:7865–7870.
10. Raskin, D., and P. de Boer. 1997. The MinE ring: an FtsZ-independent cell structure required for selection of the correct division site in *E. coli*. *Cell.* 91:685–694.
11. Hu, Z., E. Gogol, and J. Lutkenhaus. 2002. Dynamic assembly of MinD on phospholipid vesicles regulated by ATP and MinE. *Proc. Natl. Acad. Sci. USA.* 99:6761–6766.
12. Fu, X., Y. Shih, Y. Zhang, and L. Rothfield. 2001. The MinE ring required for proper placement of the division site is a mobile structure that changes its cellular location during the *Escherichia coli* division cycle. *Proc. Natl. Acad. Sci. USA.* 98:980–985.
13. Hale, C., H. Meinhardt, and P. de Boer. 2001. Dynamic localization cycle of the cell division regulator MinE in *Escherichia coli*. *EMBO J.* 20:1563–1572.
14. Meinhardt, H., and P. de Boer. 2001. Pattern formation in *Escherichia coli*: a model for the pole-to-pole oscillations of Min proteins and the localization of the division site. *Proc. Natl. Acad. Sci. USA.* 98:14202–14207.
15. Howard, M., A. Rutenberg, and S. de Vet. 2001. Dynamic compartmentalization of bacteria: accurate division in *E. coli*. *Phys. Rev. Lett.* 87:278102.
16. Kruse, K. 2002. A dynamic model for determining the middle of *Escherichia coli*. *Biophys. J.* 82:618–627.
17. Huang, K., Y. Meir, and N. Wingreen. 2003. Dynamic structures in *Escherichia coli*: spontaneous formation of MinE rings and MinD polar zones. *Proc. Natl. Acad. Sci. USA.* 100:12724–12728.
18. Howard, M., and A. Rutenberg. 2003. Pattern formation inside bacteria: fluctuations due to the low copy number of proteins. *Phys. Rev. Lett.* 90:128102.
19. Huang, K., and N. Wingreen. 2004. Min-protein oscillations in round bacteria. *Phys. Biol.* 1:229–235.
20. Meacci, G., and K. Kruse. 2005. Min-oscillations in *Escherichia coli* induced by interactions of membrane-bound proteins. *Phys. Biol.* 2:89–97.
21. Kerr, R., H. Levine, T. Sejnowski, and W. Rappel. 2006. Division accuracy in a stochastic model of Min oscillations in *Escherichia coli*. *Proc. Natl. Acad. Sci. USA.* 103:347–352.
22. Pavin, N., H. Paljetak, and V. Krstic. 2006. Min-protein oscillations in *Escherichia coli* with spontaneous formation of two-stranded filaments in a three-dimensional stochastic reaction-diffusion model. *Phys. Rev. E Stat. Nonlin. Soft Matter Phys.* 73:021904.
23. Tostevin, F., and M. Howard. 2006. A stochastic model of Min oscillations in *Escherichia coli* and Min protein segregation during cell division. *Phys. Biol.* 3:1–12.
24. Shih, Y., X. Fu, G. King, T. Le, and L. Rothfield. 2002. Division site placement in *E. coli*: mutations that prevent formation of the MinE ring lead to loss of the normal midcell arrest of growth of polar MinD membrane domains. *EMBO J.* 21:3347–3357.
25. Suefuji, K., R. Valluzzi, and D. R. Chaudhuri. 2002. Dynamic assembly of MinD into filament bundles modulated by ATP, phospholipids, and MinE. *Proc. Natl. Acad. Sci. USA.* 99:16776–16781.

26. Drew, D., M. Osborn, and L. Rothfield. 2005. A polymerization-depolymerization model that accurately generates the self-sustained oscillatory system involved in bacterial division site placement. *Proc. Natl. Acad. Sci. USA*. 102:6114–6118.

27. Norris, V., C. Woldringh, and E. Mileykovskaya. 2004. A hypothesis to explain division site selection in *Escherichia coli* by combining nucleoid occlusion and Min. *FEBS Lett*. 561:3–10.

28. Mileykovskaya, E., and W. Dowhan. 2000. Visualization of phospholipid domains in *Escherichia coli* by using the cardiolipin-specific fluorescent dye 10-*n*-nonyl acridine orange. *J. Bacteriol*. 182:1172–1175.

29. Mileykovskaya, E., I. Fishov, X. Fu, B. Corbin, W. Margolin, and W. Dowhan. 2003. Effects of phospholipid composition on MinD-membrane interactions in vitro and in vivo. *J. Biol. Chem*. 278:22193–22198.

30. Fange, D., and J. Elf. 2006. Noise-induced Min phenotypes in *E. coli*. *PLoS Comput. Biol*. 2:e80.

31. Kenworthy, A., B. Nichols, C. Remmert, G. Hendrix, M. Kumar, J. Zimmerberg, and J. Lippincott-Schwartz. 2004. Dynamics of putative raft-associated proteins at the cell surface. *J. Cell Biol*. 165:735–746.

32. Lackner, L., D. Raskin, and P. de Boer. 2003. ATP-dependent interactions between *Escherichia coli* Min proteins and the phospholipid membrane in vitro. *J. Bacteriol*. 185:735–749.

33. Holy, T., and S. Leibler. 1994. Dynamic instability of microtubules as an efficient way to search in space. *Proc. Natl. Acad. Sci. USA*. 91: 5682–5685.

34. Hu, Z., C. Saez, and J. Lutkenhaus. 2003. Recruitment of MinC, an inhibitor of Z-ring formation, to the membrane in *Escherichia coli*: role of MinD and MinE. *J. Bacteriol*. 185:196–203.

35. de Boer, P., R. Crossley, A. Hand, and L. Rothfield. 1991. The MinD protein is a membrane ATPase required for the correct placement of the *Escherichia coli* division site. *EMBO J*. 10:4371–4380.

36. Zhang, Y., S. Rowland, G. King, E. Braswell, and L. Rothfield. 1998. The relationship between hetero-oligomer formation and function of the topological specificity domain of the *Escherichia coli* MinE protein. *Mol. Microbiol*. 30:265–273.

37. Szeto, T., S. Rowland, L. Rothfield, and G. King. 2002. Membrane localization of MinD is mediated by a C-terminal motif that is conserved across eubacteria, archaea, and chloroplasts. *Proc. Natl. Acad. Sci. USA*. 99:15693–15698.

38. Hu, Z., and J. Lutkenhaus. 2003. A conserved sequence at the C-terminus of MinD is required for binding to the membrane and targeting MinC to the septum. *Mol. Microbiol*. 47:345–355.

39. Lutkenhaus, J., and M. Sundaramoorthy. 2003. MinD and role of the deviant Walker A motif, dimerization and membrane binding in oscillation. *Mol. Microbiol*. 48:295–303.

40. Sweitzer, S., and J. Hinshaw. 1998. Dynamin undergoes a GTP-dependent conformational change causing vesiculation. *Cell*. 93:1021–1029.

41. Fygenson, D., J. Marko, and A. Libchaber. 1997. Mechanics of microtubule-based membrane extension. *Phys. Rev. Lett*. 79:44974500.

42. Bo, L., and R. Waugh. 1989. Determination of bilayer membrane bending stiffness by tether formation from giant, thin-walled vesicles. *Biophys. J*. 55:509–517.

43. Huang, K., R. Mukhopadhyay, and N. Wingreen. 2006. A curvature-mediated mechanism for localization of lipids to bacterial poles. *PLoS Comput. Biol*. 2:e151.

44. Lipowsky, R., and R. Dimova. 2003. Domains in membranes and vesicles. *J. Phys. Cond. Matter*. 15:S31–S45.

45. Edelstein-Keshet, L., and G. Ermentrout. 1998. Models for the length distributions of actin filaments: I. Simple polymerization and fragmentation. *Bull. Math. Biol*. 60:449–475.

46. Fygenson, D., H. Flyvbjerg, K. Sneppen, A. Libchaber, and S. Leibler. 1995. Spontaneous nucleation of microtubules. *Phys. Rev. E Stat. Nonlin. Soft Matter. Phys*. 51:5058–5063.

47. Zhao, C., P. de Boer, and L. Rothfield. 1995. Proper placement of the *Escherichia coli* division site requires two functions that are associated with different domains of the MinE protein. *Proc. Natl. Acad. Sci. USA*. 92:4313–4317.

48. Pichoff, S., B. Vollrath, C. Touriol, and J. Bouche. 1995. Deletion analysis of gene minE which encodes the topological specificity factor of cell division in *Escherichia coli*. *Mol. Microbiol*. 18:321–329.

49. King, G., Y. Shih, M. Maciejewski, N. Bains, B. Pan, S. Rowland, G. Mullen, and L. Rothfield. 2000. Structural basis for the topological specificity function of MinE. *Nat. Struct. Biol*. 7:1013–1017.

50. Zhou, H., R. Schulze, S. Cox, C. Saez, Z. Hu, and J. Lutkenhaus. 2005. Analysis of MinD mutations reveals residues required for MinE stimulation of the MinD ATPase and residues required for MinC interaction. *J. Bacteriol*. 187:629–638.

51. Ma, L., G. King, and L. Rothfield. 2004. Positioning of the MinE binding site on the MinD surface suggests a plausible mechanism for activation of the *Escherichia coli* MinD ATPase during division site selection. *Mol. Microbiol*. 54:99–108.

52. Szeto, J., N. Eng, S. Acharya, M. Rigden, and J. Dillon. 2005. A conserved polar region in the cell division site determinant MinD is required for responding to MinE-induced oscillation but not for localization within coiled arrays. *Res. Microbiol*. 156:17–29.

53. Hayashi, I., T. Oyama, and K. Morikawa. 2001. Structural and functional studies of MinD ATPase: implications for the molecular recognition of the bacterial cell division apparatus. *EMBO J*. 20:1819–1828.

54. Howard, J. 2001. Mechanics of Motor Proteins and the Cytoskeleton. Sinauer Associates, Sunderland, MA.

55. Wollman, R., E. Cytrynbaum, J. Jones, T. Meyer, J. Scholey, and A. Mogilner. 2005. Efficient chromosome capture requires a bias in the ''search-and-capture'' process during mitotic-spindle assembly. *Curr. Biol*. 15:828–832.

56. Rowland, S., X. Fu, M. Sayed, Y. Zhang, W. Cook, and L. Rothfield. 2000. Membrane redistribution of the *Escherichia coli* MinD protein induced by MinE. *J. Bacteriol*. 182:613–619.

57. VanBuren, V., L. Cassimeris, and D. Odde. 2005. Mechanochemical model of microtubule structure and self-assembly kinetics. *Biophys. J*. 89:2911–2926.

58. Garner, E., C. Campbell, and R. Mullins. 2004. Dynamic instability in a DNA-segregating prokaryotic actin homolog. *Science*. 306:1021–1025.

59. Gillespie, D. 1976. General method for numerically simulating stochastic time evolution of coupled chemical-reactions. *Phys. Rev. Lett*. 22:403–434.

60. Carlier, M., R. Melki, D. Pantaloni, T. Hill, and Y. Chen. 1987. Synchronous oscillations in microtubule polymerization. *Proc. Natl. Acad. Sci. USA*. 84:5257–5261.

61. Pirollet, F., D. Job, R. Margolis, and J. Garel. 1987. An oscillatory mode for microtubule assembly. *EMBO J*. 6:3247–3252.

62. Marx, A., and E. Mandelkow. 1994. A model of microtubule oscillations. *Eur. Biophys. J*. 22:405–421.

63. Sept, D., H. Limbach, H. Bolterauer, and J. Tuszynski. 1999. A chemical kinetics model for microtubule oscillations. *J. Theor. Biol*. 197:77–88.

64. Gonze, D., J. Halloy, and A. Goldbeter. 2002. Robustness of circadian rhythms with respect to molecular noise. *Proc. Natl. Acad. Sci. USA*. 99:673–678.

65. Sun, Q., and W. Margolin. 2001. Influence of the nucleoid on placement of FtsZ and MinE rings in *Escherichia coli*. *J. Bacteriol*. 183:1413–1422.

66. Evans, E., and W. Rawicz. 1990. Entropy-driven tension and bending elasticity in condensed-fluid membranes. *Phys. Rev. Lett*. 64:2094–2097.

67. Fournier, L., and B. Joos. 2003. Lattice model for the kinetics of rupture of fluid bilayer membranes. *Phys. Rev. E Stat. Nonlin. Soft Matter Phys*. 67:051908.

68. Elowitz, M., M. Surette, P. Wolf, J. Stock, and S. Leibler. 1999. Protein mobility in the cytoplasm of *Escherichia coli*. *J. Bacteriol*. 181:197–203.

69. Meacci, G., J. Ries, E. Fischer-Friedrich, N. Kahya, P. Schwille, and K. Kruse. 2006. Mobility of Min-proteins in *Escherichia coli* measured by fluorescence correlation spectroscopy. *Phys. Biol*. 3:255–263.

70. Stricker, J., P. Maddox, E. Salmon, and H. Erickson. 2002. Rapid assembly dynamics of the *Escherichia coli* FtsZ-ring demonstrated by fluorescence recovery after photobleaching. *Proc. Natl. Acad. Sci. USA*. 99:3171–3175.